第 14 卷 第 2 期
2025 年 3 月
集 成 技 术
JOURNAL OF INTEGRATION TECHNOLOGY
Vol. 14 No. 2
Mar. 2025

引文格式：
王鹤然, 谢吉雄, 朱炯滔, 等. 锥形束 CT 中简单动态滤波策略的数值验证 [J]. 集成技术, 2025, 14(2): 71-85.
Wang HR, Xie JX, Zhu JT, et al. Numerical validation of a simple dynamic beam filtration strategy in cone beam CT [J]. Journal of Integration Technology, 2025, 14(2): 71-85.

锥形束 CT 中简单动态滤波策略的数值验证

王鹤然[1,2,3] 谢吉雄[3] 朱炯滔[1,3] 张 欣[1,2,3] 谭雨航[1,3] 苏 婷[1,3] 葛永帅[1,2,3,4,5*]

[1](中国科学院深圳先进技术研究院 深圳 518055)
[2](中国科学院大学 北京 100049)
[3](中国科学院深圳先进技术研究院先进探测材料与医学成像器件研究中心 深圳 518055)
[4](中国科学院深圳先进技术研究院劳特伯生物医学成像研究中心 深圳 518055)
[5](中国科学院医学成像科学与技术系统重点实验室 深圳 518055)

摘 要 对于锥束计算机断层扫描 (cone beam computed tomography，CBCT)，人们一直希望能够在扫描过程中动态地调节 X 射线的强度和分布，以适应患者内部的解剖结构。这样就可以达到减少图像伪影和降低辐射剂量的目的。然而，目前的动态滤波装置，如动态 Bowtie 滤波器，其结构较为复杂难以真正应用到临床，因此，本研究旨在设计一种结构简单的动态滤波策略，以减少 CBCT 成像中的图像伪影同时降低辐射剂量。本研究所设计的动态滤波策略随着 CBCT 的旋转而动态变化，具体而言，该动态滤波策略是将两个不同部分集成在一起：滤片部分和 Bowtie 部分。该动态滤波策略设置有两种工作模式，一种是动态滤片与动态 Bowtie 的组合，称为动态滤片-动态 Bowtie (Dynamic filter-Dynamic bowtie，DFDB)；另一种是动态滤片与静态 Bowtie 的组合，称为动态滤片-静态 Bowtie (Dynamic filter-Static bowtie，DFSB)。本研究分别针对 3 个人体部位(肩部、胸部和膝部)进行了数值仿真模拟，且使用蒙特卡罗模拟平台 MC-GPU 生成每个体模对应的剂量分布图。结果表明，使用所提出的 DFDB 和 DFSB 动态滤波方案可以显著减少图像伪影，从而改善 CBCT 图像质量。根据扫描部位的不同，辐射剂量的降低幅度达到约 30%。因此，本研究所提出的简单动态滤波策略 DFDB和 DFSB，可以有效提升图像质量同时降低辐射剂量，且拥有足够简单的结构 (尤其是 DFSB)，在一定程度上推进了动态滤波策略的临床应用。

关键词 动态滤波；辐射剂量降低；硬化伪影减少；锥束 CT
中图分类号 R814.4 **文献标志码** A doi: 10.12146/j.issn.2095-3135.20241021001
CSTR: 32239.14.j.issn.2095-3135.20241021001

收稿日期：2024-10-21 **修回日期**：2024-10-29
基金项目：国家自然科学基金项目 (12305349, 12235006, 12027812)；深圳市科技计划项目 (JSGGKQTD20210831174329010)；广东省基础与应用基础研究基金项目 ((2021TQ06Y108)
作者简介：王鹤然，硕士研究生，研究方向为新型低剂量 CT 成像技术； 谢吉雄，硕士研究生，研究方向为单光子 X 射线成像方法与器件； 朱炯滔，博士研究生，研究方向为锥束能谱 CT 成像算法； 张欣，博士研究生，研究方向为高分辨显微能谱 CT 成像； 谭雨航，中级工程师，研究方向为纳米分辨 X 射线相衬 CT 成像理论及系统； 苏婷，助理研究员，研究方向为 X 射线 CT 重建算法； 葛永帅 (通讯作者)，研究员，研究方向为 X 射线相位成像，E-mail：ys.ge@siat.ac.cn。

Numerical Validation of A Simple Dynamic Beam Filtration Strategy in Cone Beam CT

WANG Heran[1,2,3] XIE Jixiong[3] ZHU Jiongtao[1,3] ZHANG Xin[1,2,3]
TAN Yuhang[1,3] SU Ting[1,3] GE Yongshuai[1,2,3,4,5*]

[1](*Shenzhen Institutes of Advanced Technology*, *Chinese Academy of Sciences*, *Shenzhen* 518055, *China*)
[2](*University of Chinese Academy of Sciences*, *Beijing* 100049, *China*)
[3](*Research Center for Advanced Detection Materials and Medical Imaging Devices*, *Shenzhen Institutes of Advanced Technology*, *Chinese Academy of Sciences*, *Shenzhen* 518055, *China*)
[4](*Paul C. Lauterbur Research Center for Biomedical Imaging*, *Shenzhen Institutes of Advanced Technology*, *Chinese Academy of Sciences*, *Shenzhen* 518055, *China*)
[5](*Key Laboratory of Biomedical Imaging Science and System*, *Chinese Academy of Sciences*, *Shenzhen* 518055, *China*)
[*]*Corresponding Author*: *ys.ge@siat.ac.cn*

Abstract For cone beam computed tomography (CBCT), there has long been a desire to modulate the intensity and distribution of the X-rays to accommodate the patient's anatomy as the gantry rotates from one projection to another. This would reduce both image artifacts and radiation dose. However, the current beam modulation setups, such as dynamic bowtie filters, may be too complex for practical use in clinical applications. This study aimed to investigate a simplified dynamic beam filtration strategy for CBCT imaging to reduce image artifacts and radiation dose. In this study, the beam filtration was designed to vary dynamically as the CBCT gantry rotates around the object. Specifically, two distinct components were integrated: the sheet filter part and the bowtie filter part. The dynamic beam filtration setup has two working schemes, one is a combination of dynamic sheet filter and dynamic bowtie filter, denoted as dynamic filter-dynamic bowtie (DFDB); the other is a combination of dynamic sheet filter and static bowtie filter, denoted as dynamic filter-static bowtie (DFSB). Numerical imaging experiments were performed for three human body parts: the shoulder, chest, and knee. In addition, the Monte Carlo simulation platform MC-GPU was used to generate the dose distribution maps. Results showed that the proposed DFDB and DFSB beam filtration schemes can significantly reduce the image artifacts and thus improve the CBCT image quality. Depending on the scanned object, the total radiation dose could be reduced by 30%. The proposed simple dynamic beam filtration strategy, especially the DFSB approach, could be beneficial in the future to improve the CBCT image quality with reduced image artifacts and radiation dose.

Keywords dynamic filtration; radiation dose reduction; artifacts reduction; cone beam computed tomography
Funding This work was supported in part by National Natural Science Foundation of China (12305349, 12235006, 12027812), Shenzhen Science and Technology Program (JSGGKQTD20210831174329010), Guangdong Basic and Applied Basic Research Foundation (2021TQ06Y108)

1 Introduction

Over the past decades, cone beam computed tomography (CBCT) has been widely utilized in clinics for disease diagnosis, interventional surgery, and radiotherapy. However, the radiation dose

received by patients has become a significant public health concern. Consequently, there has been a significant research interest in effectively reducing radiation dose to comply with the as low as reasonably achievable (ALARA) principle. For example, reducing the total number of projections[1-2] and lowering the tube current[3-4] are two of the most efficient approaches to reduce the radiation dose. To do so, the model based iterative construction algorithm and the most advanced deep learning based image reconstruction algorithms have been investigated. On the other hand, attention has also been given to attenuating the excessive irradiation of the object during CBCT scans. By far, numerous techniques have been developed. For example, the tube current modulation (TCM) approach[5-7] dynamically modulates the emitted number of X-ray photons at different projection angles. However, the distribution of X-ray photons on the detector surface remains constant and cannot be modulated. To mitigate this, a beam filtering module shaped like a bowtie is placed between the X-ray source and the scanned object to predominantly modulate the in-plane X-ray photon distribution. With a bowtie filter[8-9], a higher attenuation is introduced on the X-ray path located far from the center of the scanned object, while a lower attenuation is introduced on the X-ray path near the center of the scanned object. Besides, the use of a bowtie filter can also reduce the beam hardening artifacts and the Compton scatter artifacts[10-11].

Usually, the shape and position of a bowtie filter are fixed as the gantry rotates. In other words, the modulation of X-ray photons by the bowtie filters remains identical at different view angles, which fails to meet the dynamic filtering requirements throughout the entire scan. Hence, in recent years, dynamic bowtie attenuators (DBA) have been proposed to alter the in-plane X-ray photon distribution. Several types of DBAs have been proposed, such as sheet-based dynamic bowtie[12-15], wedge-based dynamic bowtie[16-19], and fluid dynamic bowtie attenuators[20-22]. As demonstrated, dynamic bowtie filters are able to modulate the distribution of X-ray photons at each projection angle to generate more homogeneous CT images with lower patient dose[8,11]. Despite their promising capabilities, dynamic bowtie filters are still under investigation due to their complicated mechanical structures and precise control. For instance, the flow rate of liquids in a fluid dynamic bowtie limits its implementation. Therefore, designing some novel dynamic beam filters with relatively simple structures and easy mechanical control is crucial for real applications.

In this study, novel dynamic beam filtration strategies are proposed, see Figure 1. Specifically, the entire beam filter contains 2 distinct parts: the aluminum sheet filter part and the bowtie filter part. The curves in the bottom plot the corresponding thickness of the Al sheet filter. For the dynamic filter-dynamic bowtie (DFDB) design, the thickness of the Al sheet varies continuously. For the dynamic filter-static bowtie (DFSB) design, the thickness of the Al sheet varies stepwise. Herein, a special rotatory Al disc is assumed for DFSB. In Figure 1 (a), the bowtie filter varies its opening width and the aluminum sheet filter changes its thickness continuously as the gantry rotates. This special design is denoted as DFDB mode. As a simplified version of DFDB, the DFSB mode shown in Figure 1 (b) contains a fixed bowtie filter and a

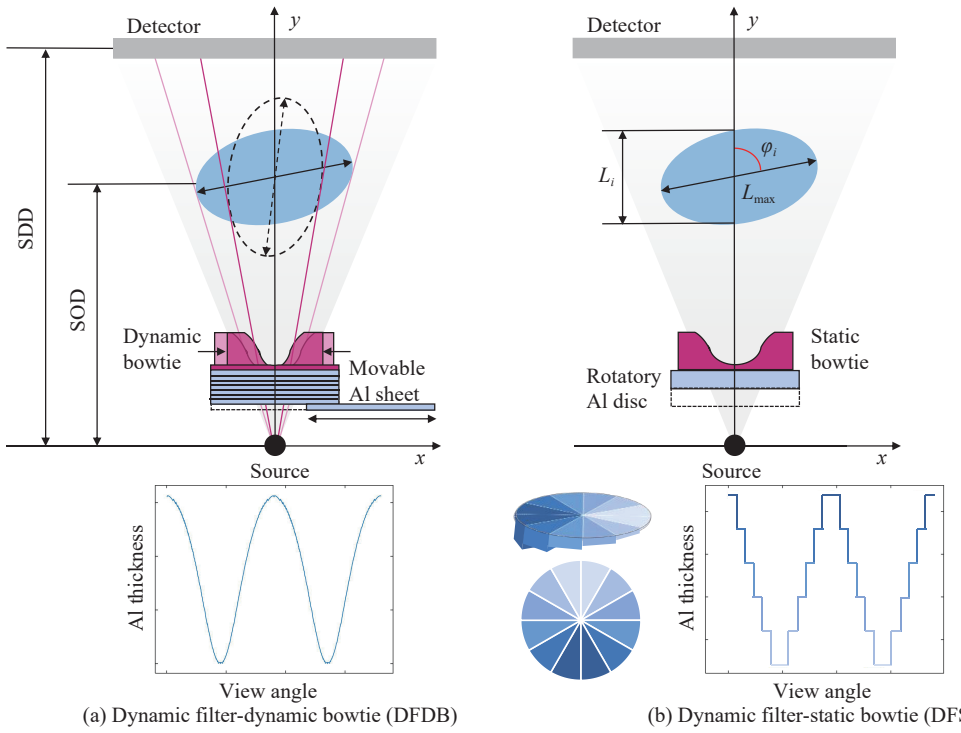

Fig. 1 Design of the dynamic filter

rotatory aluminum disc, which is composed of several stepwise aluminum sheets. Depending on the shape of the object at different projection angles, the Al disc rotates accordingly to a specific thickness location. Note that the DFSB design has a much simpler mechanical structure than the DFDB design, making it much more appropriate for practical applications. The performance of the proposed dynamic filtration strategies for CBCT imaging are investigated in terms of image quality and radiation dose reduction.

2 Methods

2.1 Design of the dynamic filter

The fundamental idea of designing the dynamic filter is to ensure that the distribution of X-ray photons on the detector plane at different angles is as uniform as possible. As a result, the irregular shapes (non-circular shapes) of the scanned object are compensated. The designed dynamic filters are shown in Figure 1. The DFDB design consists of 2 moving parts: the movable aluminum sheets and the dynamic bowtie, as shown in Figure 1 (a). The DFSB is a simplified design of the DFDB and consists of a rotatory aluminum disc and a static bowtie, as shown in Figure 1 (b). During the design, only the number of X-ray photons received by the central pixel of the detector is considered. In addition, it is assumed that the imaging object is merely composed of water.

The following approach is used to determine the required aluminum thickness L_{Ali} of the beam filter. Assume N_0 denotes the emitted number of X-ray photons for the central ray, then the number of X-ray photons after passing through the longest central path of the object ($N_{\max}$) is equal to:

$$N_{\max}=N_0\mathrm{e}^{-\mu_{\mathrm{water}}L_{\max}-\mu_{\mathrm{Al}}L_{\mathrm{Al}}} \tag{1}$$

where μ_{water} and μ_{Al} denote the linear attenuation coefficient of water and aluminum respectively at the effective beam energy; $L_{\max}$ denotes the longest central path length; and L_{Al} denotes the thickness of the aluminum in the central position of the bowtie. In addition, the number of X-ray photons at view angle φ_i after traversing the central path of the object N_i is expressed as follows:

$$N_i = N_0 \mathrm{e}^{-\mu_{\text{water}} L_i - \mu_{\text{Al}} L_{\text{Al}} - \mu_{\text{Al}} L_{\text{Ali}}} \tag{2}$$

in which L_i denotes the length of the center path of the object at the view angle φ_i; L_{Ali} denotes the required thickness of the aluminum at the view angle φ_i. In order to determine L_{Ali}, $N_i = N_{\max}$ is assumed. Immediately,

$$L_{\text{Ali}} = \mu_{\text{water}}/\mu_{\text{Al}} \times (L_{\max} - L_i) \tag{3}$$

Note that $L_i = L_{\max}$ when the view angle corresponds to the longest center path. Consequently, the total thickness of the added aluminum is 0.

In DFDB, the bowtie filter moves dynamically. It consists of 3 components: a base and 2 aluminum blocks that can move back and forth on the base. The movements of these 2 blocks depend on the 2 X-rays that are tangent to the central section of the phantom, as shown in Figure 1 (a). This ensures that the left and right tangents always intersect with the left and right blocks at the 1/3 position of the block from the top edge, respectively. And the movable aluminum sheets can achieve any required thickness by increasing or decreasing their quantity. In DFSB, the bowtie filter does not move, and the rotatory aluminum disc is assumed to be divided into 12 pieces, each covering 30 degrees. The first 6 pieces transition from thin to thick, followed by 6 pieces transitioning from thick to thin. A complete rotation corresponds to a cycle of thickness that goes from thin to thick and then back to thin during the CBCT scan. By design, the rotation speed of the aluminum disc is set to twice the rotation speed of the CBCT. The thinnest part of the aluminum disc is set to 0.2 cm, while the thickest part is approximated to the calculated maximum aluminum thickness (rounded down to the nearest 0.1 cm), and the remaining pieces of the disc are then evenly spaced.

2.2 Phantoms

In total, 3 clinical CT imaging data were employed in this study, see Figure 2. They were downloaded from The Cancer Imaging Archive (TCIA) (www.cancerimagingarchive.net). As shown in Figure 2, the thickness of the aluminum sheets changed continuously in DFDB, while it changed stepwise in DFSB. The forward projection and the CT reconstruction (using the filter back projection (FBP) method) were performed using Python (version 3.8). More details of the simulations are listed in Table 1.

2.3 Simulation method

Monte Carlo simulations were performed to estimate the dose distribution. The MC-GPU v1.3 package[23] was used. To take the variations of the dynamic filter into account in MC-GPU, the object and the dynamic filter at each angle were combined in advance. Afterward, these combined results were sequentially fed into the MC-GPU to generate the dose distribution maps at each angle.

The geometry used in MC-GPU simulations is the same as listed in Table 1. The X-ray tube, phantom, and detector were positioned so that the projection of the focal spot through the center of the phantom coincided with the center of the detector. In total, 1.2×10^9 number of X-ray photons were assumed per projection, and 720 projections over

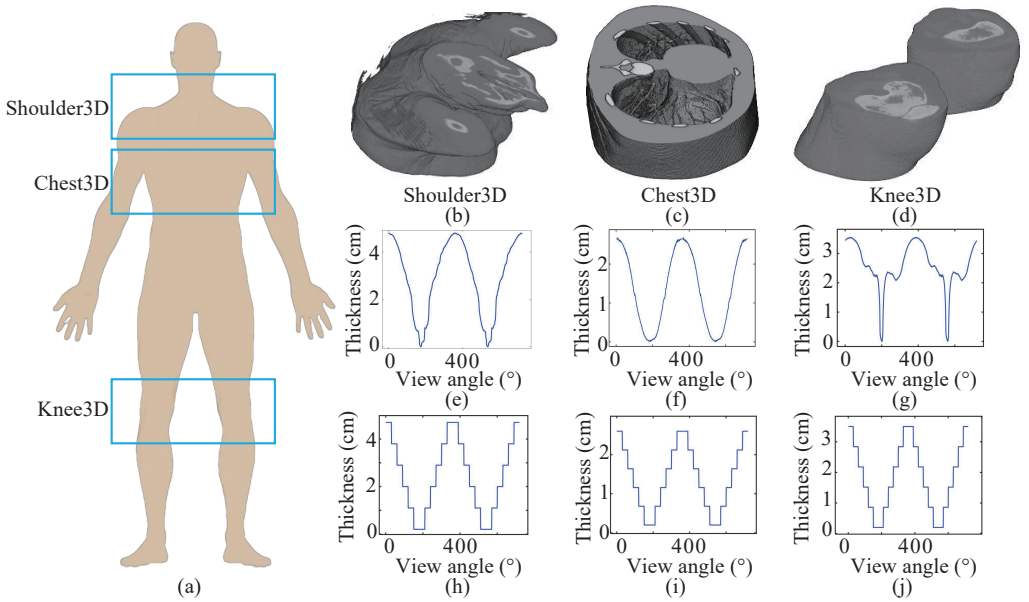

Fig. 2 Three body parts were imaged in this study (a), including the shoulder, denoted as Shoulder3D (b), the chest, denoted as Chest3D (c), and the knee, denoted as Knee3D (d). The corresponding thickness of the aluminum sheet for DFDB at each view angle are plotted in (e), (f), and (g), respectively. Meanwhile, the required thickness of the aluminum disc for DFSB at each view angle are plotted in (h), (i), and (j), respectively

Table 1 Key parameters used in simulations

Parameter	Value
Source trajectory	Full circle
Source to object distance (SOD)	115.63 cm
Source to detector distance (SDD)	156.06 cm
Total views (n)	720
Source to bowtie distance	10 cm
Static bowtie thickness	6 cm
Bowtie central thickness (L_{Al})	1 cm
Image matrix	512×512×100
Voxel size	0.8×0.8×0.8 mm^3
Detector array	1 620×360
Detector pixel size	0.417×0.417 mm^2
Tube voltage	120 kVp
Inherent beam filter	Al: 5 mm, Cu: 0.2 mm

360° were simulated.

Besides the DFDB and DFSB settings, 3 other settings were also simulated for comparisons: No-bowtie, tube current modulation (TCM), and static bowtie (SB). Specifically, the tube modulation factor (TMF) for view angle φ_i is defined[5,24] as:

$$\mathrm{TMF}_i = \sqrt{A_i} / \sum_i^n \sqrt{A_i} \tag{4}$$

where $A_i = N_0 / N_i$ denotes the central path primary

attenuation of the view angle φ_i; N_0 denotes the emitted number of X-ray photons; N_i denotes the number of photons detected by the central detector at view angle φ_i and n denotes the total number of projections. Moreover, the SB is the same as the one used in DFSB.

The numerical simulations were conducted separately for different body parts. It was believed that it is important to maintain the image SNR while reducing the beam hardening artifacts and radiation dose. Therefore, it was assumed that the total number of photons received by the central detector remains constant for different beam filtration settings within a full CBCT scan. This ensures that the signal-to-noise ratios (SNRs) of the final reconstructed CBCT images from different filtration settings are approximately the same.

3 Results

3.1 Imaging results

The imaging results of the Shoulder3D are shown in Figure 3. From top to bottom, the images correspond to different settings: no-bowtie, TCM, SB, DFDB, and DFSB. From left to right, the images correspond to different anatomical structures. The scale bar denotes 5 cm. As indicated by the arrows, the beam hardening artifacts are quite severe in the top 3 rows. The proposed DFDB and DFSB can significantly reduce the hardening artifacts in the shoulder region, thus resulting in more uniform CT images.

The imaging results of the Chest3D are shown in Figure 4. Compared to the no-bowtie, TCM, and SB settings, the DFDB and DFSB approaches are able to significantly reduce the hardening image artifacts in the areas highlighted by the arrows, resulting in more uniform CT images. Therefore, it is demonstrated that the proposed DFDB and DFSB strategies can greatly improve the overall quality of reconstructed CT images.

The imaging results of the Knee3D are shown in Figure 5. Similar to the results obtained previously, both DFDB and DFSB can greatly reduce beam hardening artifacts, making the tissues clearly visible. This result indicates that DFDB and DFSB can also be used to scan 2 or more disconnected parts. In all, the imaging results of the 3 models clearly demonstrate that the proposed DFDB and DFSB can effectively reduce beam hardening artifacts and thus improve the image quality.

The SNR values of different body parts under various situations are plotted in Figure 6. 3 regions of interest (ROI) were highlighted with yellow circles in Figure 3- Figure 5. It can be seen that the variation in SNR is minimal, indicating that the SNR is well maintained for each imaging scenario. It is believed that it is important to keep the SNR similar while discussing the reduction of image artifacts and radiation dose.

3.2 Dose results

The dose distribution maps of the Shoulder3D for the 5 different beam filtration settings are shown in Figure 7. From top to bottom, results correspond to different settings: no-bowtie, TCM, SB, DFDB, and DFSB. From left to right, results correspond to different anatomical structures. The blue dashed line outlines the 2.0 mGy dose contour. As observed, the dose reductions with DFDB and DFSB are particularly in the central region. These results indicate that DFDB and DFSB approaches can

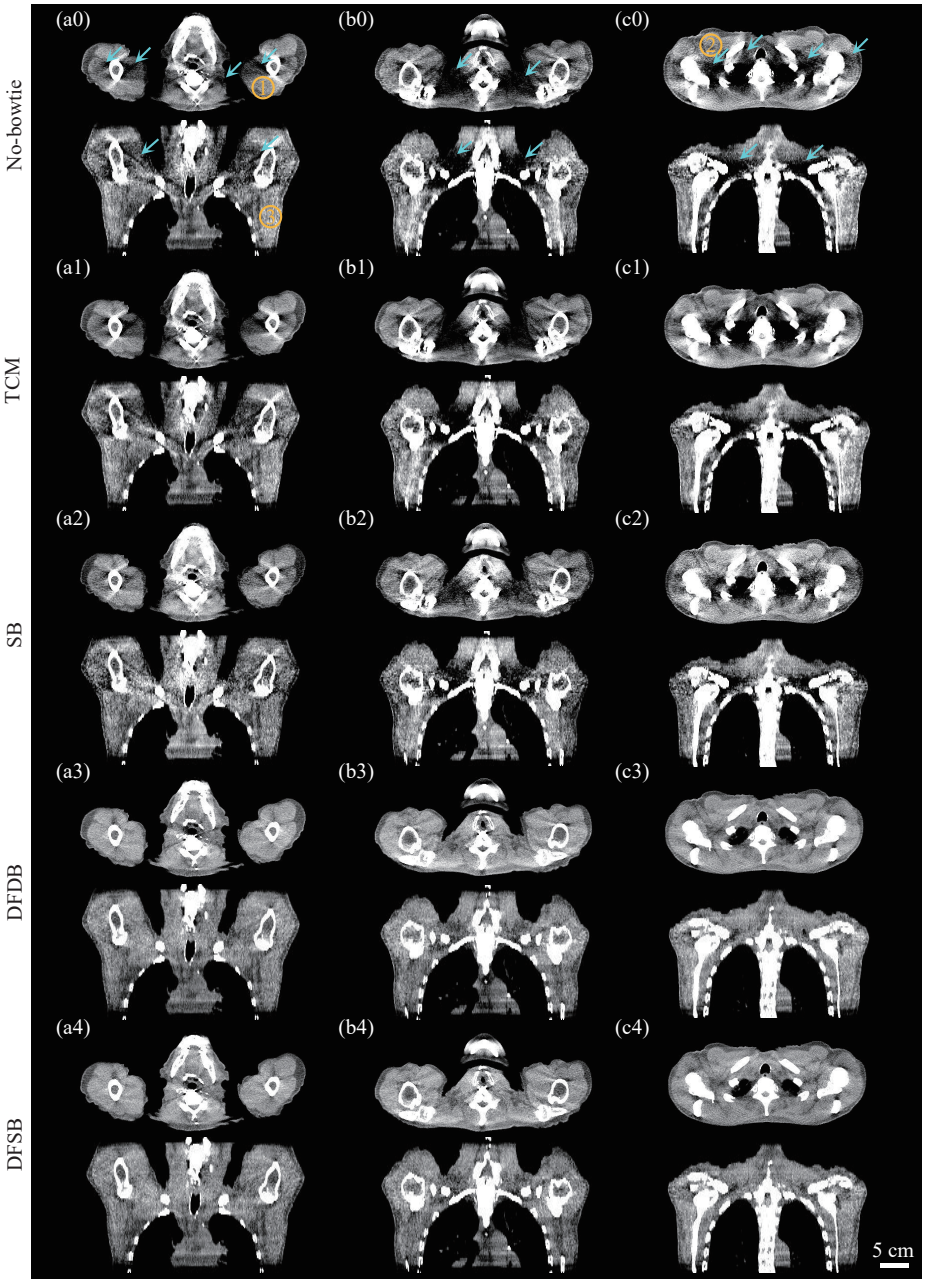

Fig. 3 Results of the Shoulder3D

reduce the radiation dose more efficiently than TCM and SB. It is demonstrated that the DFDB is more efficient in reducing the radiation dose than the DFSB.

The dose distribution maps for the Chest3D are presented in Figure 8. And the dose distribution maps for the Knee3D are presented in Figure 9. The blue dashed line outlines the 2 mGy dose contour and 2.5 mGy dose contour respectively. From these obtained dose maps, it can be clearly seen that the DFDB and DFSB can greatly increase the area of lower dose distribution compared to other beam filtration settings. Namely, the area inside the blue dashed line expands, indicating a reduction of

Fig. 4　Results of the Chest3D

radiation dose. Moreover, as expected the dose reduction by the ideal DFDB design is more than the approximated DFSB design.

In addition to the dose distribution maps, the total radiation doses are also investigated, see Table 2. In it, the relative total doses of Shoulder3D, Chest3D, and Knee3D are compared for different filtration settings. The dose level with the no-bowtie setting is referred to as 1. As shown, the overall doses received by the Shoulder3D, Chest3D, and Knee3D are reduced by 12.52%, 5.45%, and 3.17% when SB is used. They are reduced by 26.15%, 14.56% and 19.73% with the DFDB setting, correspondingly. While using DFSB, the overall dose reductions become 18.69%, 11.84% and 13.16%, respectively. However, it is found that the

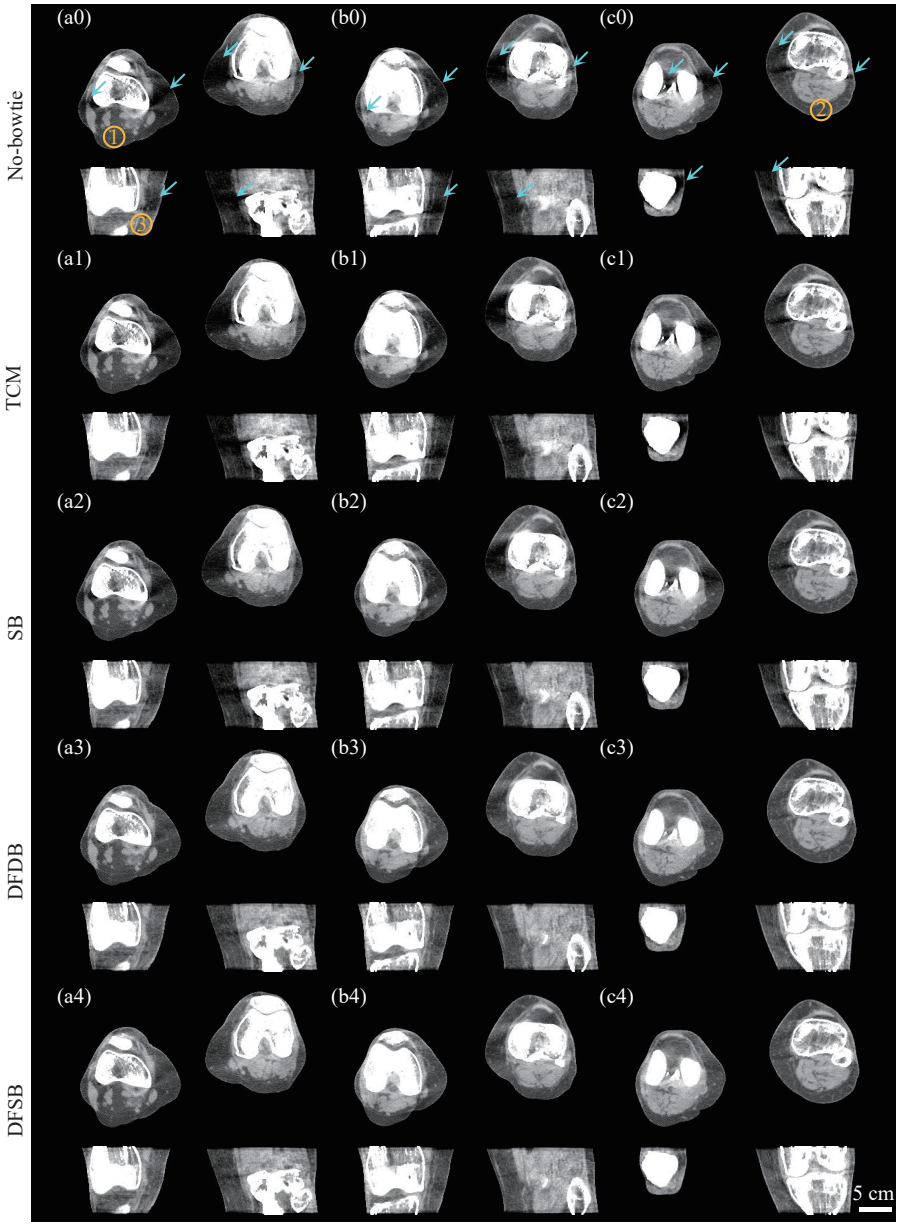

Fig. 5 Results of the Knee3D

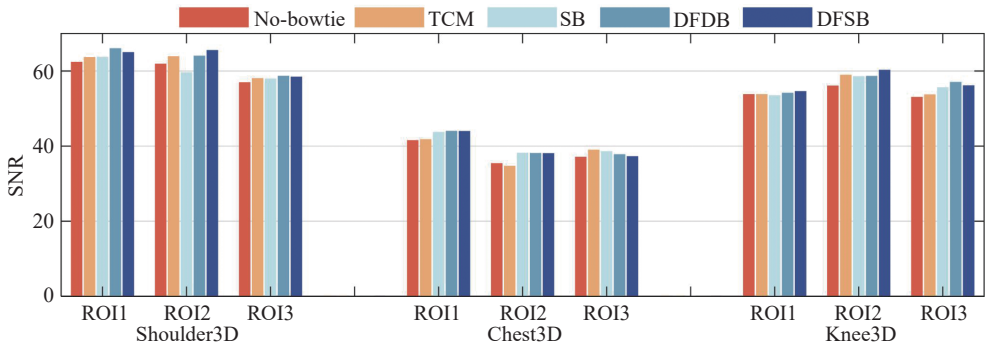

Fig. 6 The measured SNRs of different body parts

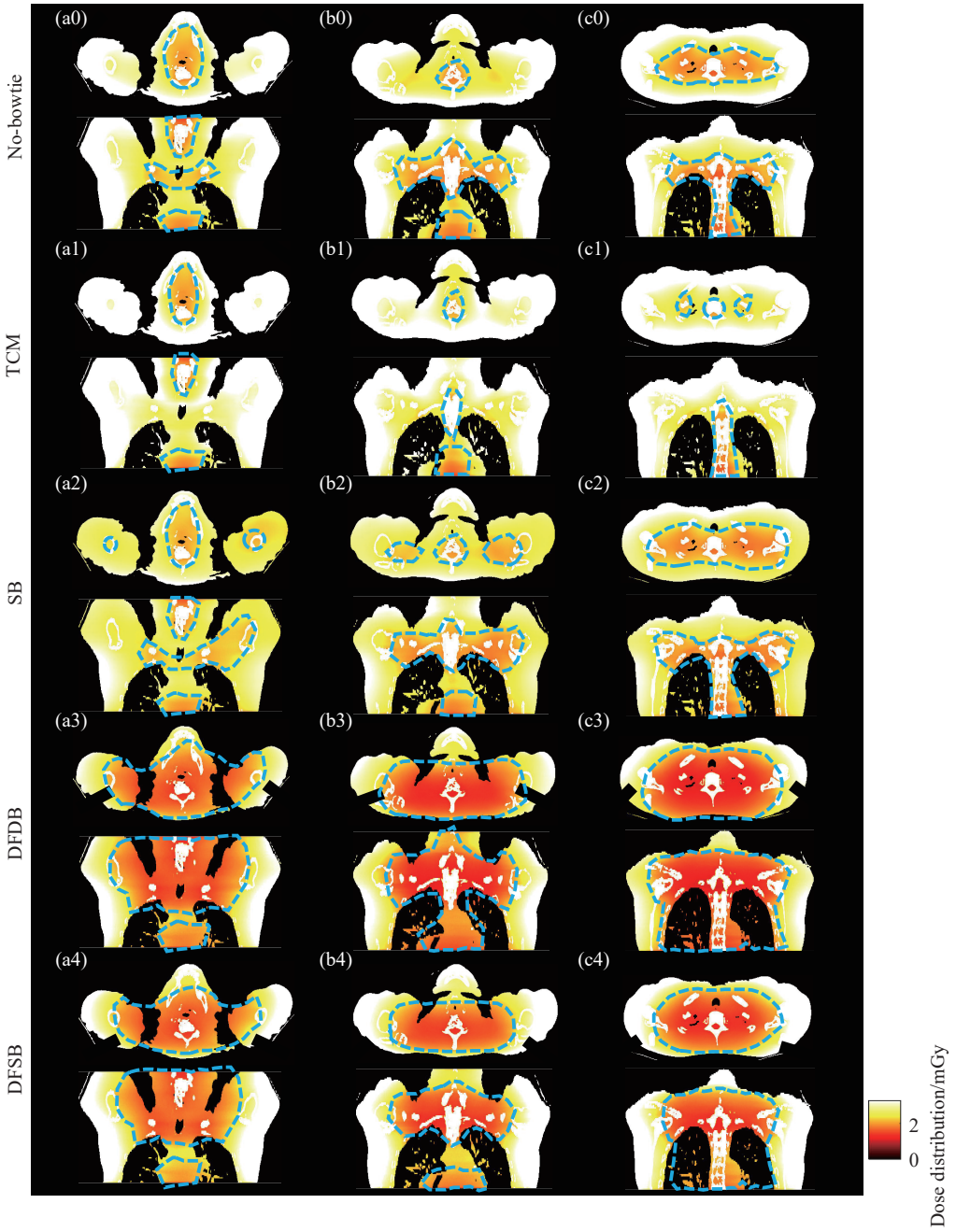

Fig. 7　The dose distribution maps of the Shoulder3D

average dose does not significantly change with the TCM setting. This is because TCM only redistributes the angular amount of emitted X-ray photons but does not reduce the spectrum of X-ray. Note that the dose levels used in this study may be different from the actual clinical applications. Regardless, the results found in this study are completely independent of the absolute dose levels.

4　Discussion and Conclusion

This study proposed a simple dynamic beam

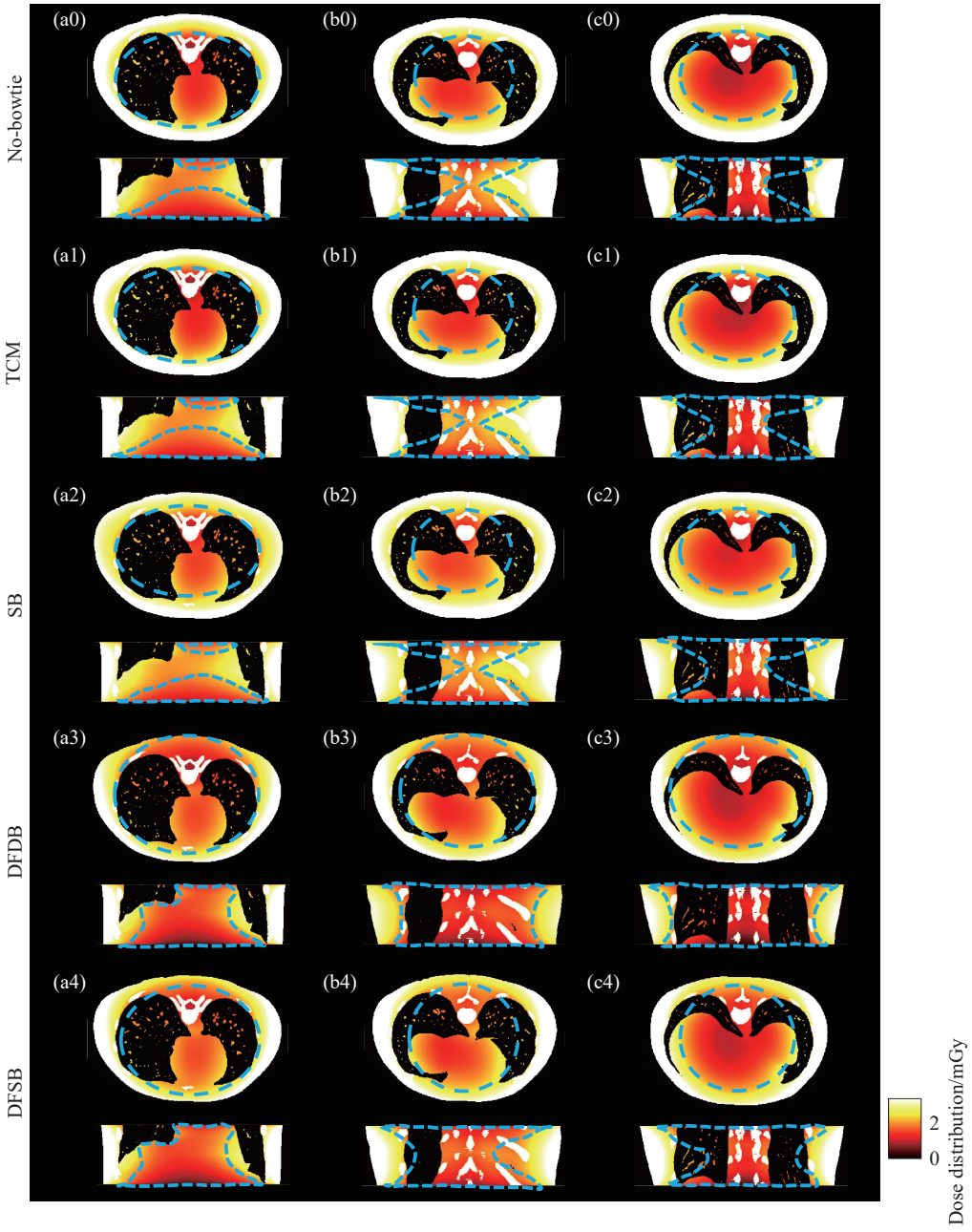

Fig. 8 The dose distribution maps of the Chest3D

filtration strategy in CBCT imaging with the purpose of enhancing the image quality while reducing the radiation dose. To avoid the complicated mechanical movements and controls associated with the dynamic bowtie filter strategy, this study only considers the mismatches in the center line path between different projection angles, rather than within a single projection angle. In a sense, the newly proposed dynamic beam filtration strategy is an approximation of the more precise dynamic bowtie filter strategy. By doing so, the design of the dynamic beam filter can be greatly simplified, and so do the mechanical movements and controls. Specifically, 2 distinct parts are integrated: the part near the scanned object

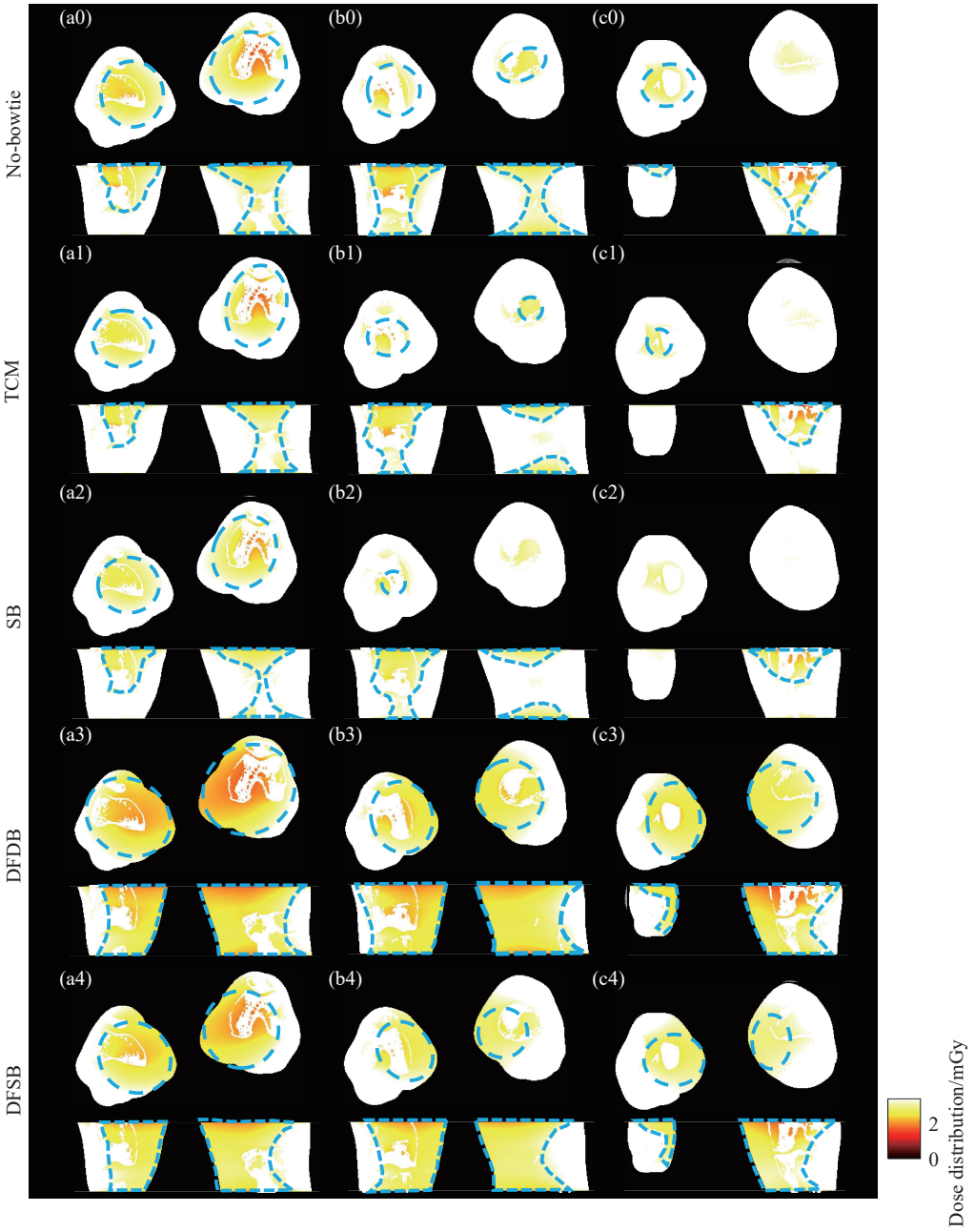

Fig. 9　The dose distribution maps of the Knee3D

is a bowtie filter, and the part near the source is composed of multiple movable aluminum sheets or a rotary aluminum disc. In particular, 2 different beam filtration schemes are proposed in this study. In addition, numerical experiments are performed to 3 clinical CT imaging data. Monte Carlo simulations were used to generate the dose distribution maps. A series of comparison studies were conducted to investigate artifact reduction and radiation dose reduction performance: no-bowtie, TCM[5-6,24], SB, DFDB, and DFSB. The DFDB and DFSB proposed in this study dynamically adjust the thickness of the filter section based on the scanning angle to increase or decrease the number of photons. This is similar to

Table 2 The absorbed total radiation dose in the human bodies under different imaging settings

Setting	Shoulder3D	Chest3D	Knee3D
No-bowtie	1	1	1
TCM	1.087 8	1.008 0	1.049 0
SB	0.874 8	0.945 5	0.968 3
DFDB	0.738 5	0.854 4	0.802 7
DFSB	0.813 1	0.881 6	0.868 4

how TCM dynamically changes the photon count according to different scanning angles. Therefore, this study compared the image and dose results of the proposed DFDB and DFSB with TCM. Results demonstrate that the DFDB and DFSB proposed in this study not only can reduce the streaking image artifacts but also can lower the radiation dose. Compared to TCM, the radiation dose can be reduced by up to 30%.

The current study may have some limitations. First, the design of the dynamic beam filter, e.g., DFDB and DFSB, is based on the assumption of a uniform water object. Namely, it is assumed that the object is pure water and the internal variations are ignored. For human body CBCT imaging, no doubt this is a good approximation. If the main composition of the scanned object changes into other material, e.g., bone or aluminum, for some particular applications, the above water assumption definitely should be altered accordingly. Second, the influence of DFDB or DFSB on the Compton scatter has not been investigated yet. We plan to investigate this phenomenon from experiments in the future with a CBCT scanner prototype installed with DFDB or DFSB. Additionally, the image artifact reduction capability, as well as the dose reduction capability, can all be validated in practice with such a prototype. Third, it is worthwhile to explore the combination of the dynamic beam filter with the TCM technique. This would achieve more efficient modulation of the X-ray flux and beam spectrum at different projection angles. As a result, the image quality and dose reduction can be further enhanced. Fourth, the proposed dynamic beam filtration strategy does not apply to multi-detector CT (MDCT) scanners because their rotation speeds are too fast (faster than 1 rps). On the contrary, the proposed strategy is more compatible with CBCT scanners, whose rotation speeds are much slower (between 0.025 rps to 0.1 rps). Fifth, no experiments were conducted with a real dynamic beam filtration device due to the lack of such hardware in our laboratory. In the future, we are interested in designing a dynamic beam filtration prototype and investigating its practical performance in artifact reduction and dose reduction on a CBCT scanner.

In conclusion, this study demonstrates the feasibility of using a simple dynamic beaming filtration strategy to greatly enhance the CT image quality and reduce the radiation dose.

References

[1] Bian J, Siewerdsen JH, Han X, et al. Evaluation of sparse-view reconstruction from flat-panel-detector cone-beam CT [J]. Physics in Medicine & Biology, 2010, 55(22): 6575.

[2] Hu Z, Gao J, Zhang N, et al. An improved statistical iterative algorithm for sparse-view and limited-

angle CT image reconstruction [J]. Scientific Reports, 2017, 7(1): 10747.

[3] Mayo JR, Hartman TE, Lee KS, et al. CT of the chest: minimal tube current required for good image quality with the least radiation dose [J]. American Journal of Roentgenology, 1995, 164(3): 603-607.

[4] Kidoh M, Nakaura T, Nakamura S, et al. Low-dose abdominal CT: comparison of low tube voltage with moderate-level iterative reconstruction and standard tube voltage, low tube current with high-level iterative reconstruction [J]. Clinical Radiology, 2013, 68(10): 1008-1015.

[5] Gies M, Kalender WA, Wolf H, et al. Dose reduction in CT by anatomically adapted tube current modulation. I. Simulation studies [J]. Medical Physics, 1999, 26(11): 2235-2247.

[6] Kalender WA, Wolf H, Suess C. Dose reduction in CT by anatomically adapted tube current modulation. II. Phantom measurements [J]. Medical Physics, 1999, 26(11): 2248-2253.

[7] Kalra MK, Maher MM, Toth TL, et al. Techniques and applications of automatic tube current modulation for CT [J]. Radiology, 2004, 233(3): 649-657.

[8] Bootsma GJ, Verhaegen F, Jaffray DA. The effects of compensator and imaging geometry on the distribution of X-ray scatter in CBCT [J]. Medical Physics, 2011, 38(2): 897-914.

[9] Graham SA, Moseley DJ, Siewerdsen JH, et al. Compensators for dose and scatter management in cone-beam computed tomography [J]. Medical Physics, 2007, 34(7): 2691-2703.

[10] Lopez-Rendon X, Zhang G, Bosmans H, et al. Beam hardening and partial beam hardening of the bowtie filter: effects on dosimetric applications in CT [C] // Proceedings of the Medical Imaging 2014: Physics of Medical Imaging, 2014, 9033: 1142-1152.

[11] Mail N, Moseley DJ, Siewerdsen JH, et al. The influence of bowtie filtration on cone-beam CT image quality [J]. Medical Physics, 2009, 36(1): 22-32.

[12] Huck SM, Fung GSK, Parodi K, et al. On the potential of ROI imaging in X-ray CT–A comparison of novel dynamic beam attenuators with current technology [J]. Medical Physics, 2021, 48(7): 3479-3499.

[13] HuckSM, Fung GSK, Parodi K, et al. The z-sbDBA, a new concept for a dynamic sheet-based fluence field modulator in X-ray CT [J]. Medical Physics, 2020, 47(10): 4827-4837.

[14] HuckSM, Fung GSK, Parodi K, et al. Sheet-based dynamic beam attenuator–a novel concept for dynamic fluence field modulation in X-ray CT [J]. Medical Physics, 2019, 46(12): 5528-5537.

[15] HuckSM, Fung GSK, Parodi K, et al. A new concept for fluence field modulation in X-ray CT: the z-sbDBA [C] // Proceedings of the Medical Imaging 2020: Physics of Medical Imaging, 2020, 11312: 1131202.

[16] Hsieh SS, Pelc NJ. The feasibility of a piecewise-linear dynamic bowtie filter [J]. Medical Physics, 2013, 40(3): 031910.

[17] Hsieh SS, Peng MV, May CA, et al. A prototype piecewise-linear dynamic attenuator [J]. Physics in Medicine & Biology, 2016, 61(13): 4974.

[18] Szczykutowicz TP, Mistretta CA. Design of a digital beam attenuation system for computed tomography: part I. system design and simulation framework [J]. Medical Physics, 2013, 40(2): 021905.

[19] Szczykutowicz TP, Mistretta CA. Experimental realization of fluence field modulated CT using digital beam attenuation [J]. Physics in Medicine & Biology, 2014, 59(5): 1305.

[20] Hermus J R, Szczykutowicz T P. Two-dimensional dynamic fluid bowtie attenuators [J]. Journal of Medical Imaging, 2016, 3(1): 013502.

[21] Shunhavanich P, Hsieh SS, Pelc NJ. Fluid-filled dynamic bowtie filter: a feasibility study [C] // Proceedings of the Medical Imaging 2015: Physics of Medical Imaging, 2015, 9412: 399-406.

[22] Shunhavanich P, Hsieh SS, Pelc NJ. Fluid-filled dynamic bowtie filter: description and comparison with other modulators [J]. Medical Physics, 2019, 46(1): 127-139.

[23] Badal A, Badano A. Accelerating Monte Carlo simulations of photon transport in a voxelized geometry using a massively parallel graphics processing unit [J]. Medical physics, 2009, 36(11): 4878-4880.

[24] Stankovic U, Ploeger LS, Sonke JJ. Improving linac integrated cone beam computed tomography image quality using tube current modulation [J]. Medical Physics, 2021, 48(4): 1739-1749.